Heterodyne Staring Array Active Imager (HSAAI)

HSAAI is a laser range-gated imager that provides all weather imaging plus range to all objects in the field of view. Figure 1 illustrates the major parts. Light from a laser diode is spectrally filtered into a number of wavebands by an array of ring resonators. The array of radiators are Bragg Gratings. Light for the local oscillators is fiber optically coupled to the receiver array. On the receiver array, light is coupled into waveguides by Bragg Gratings and heterodyne detected in a photo detector.

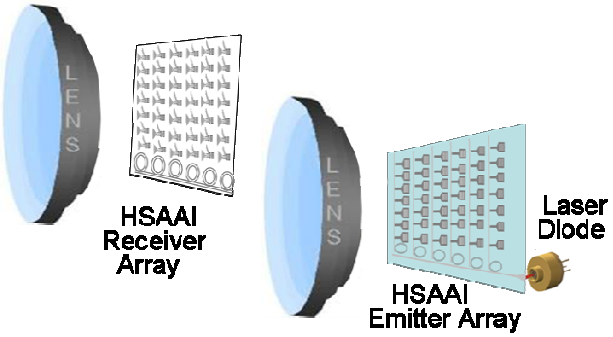

Like other active imagers, HSAAI enhances vision through rain, fog, smoke, and other atmospheric obscurants. Like other active imagers, HSAAI also provides range to all the objects in the imager field of view each frame. Unlike other active imagers, HSAAI enhances poor weather vision over very long range gates. In Figure 2, (a) shows imaging with a search light, (b) illustrates a searchlight in fog, (c) is HSAAI on a clear night, and (d) shows a HSAAI image in fog. Note that the range gate in (d) is quite long.

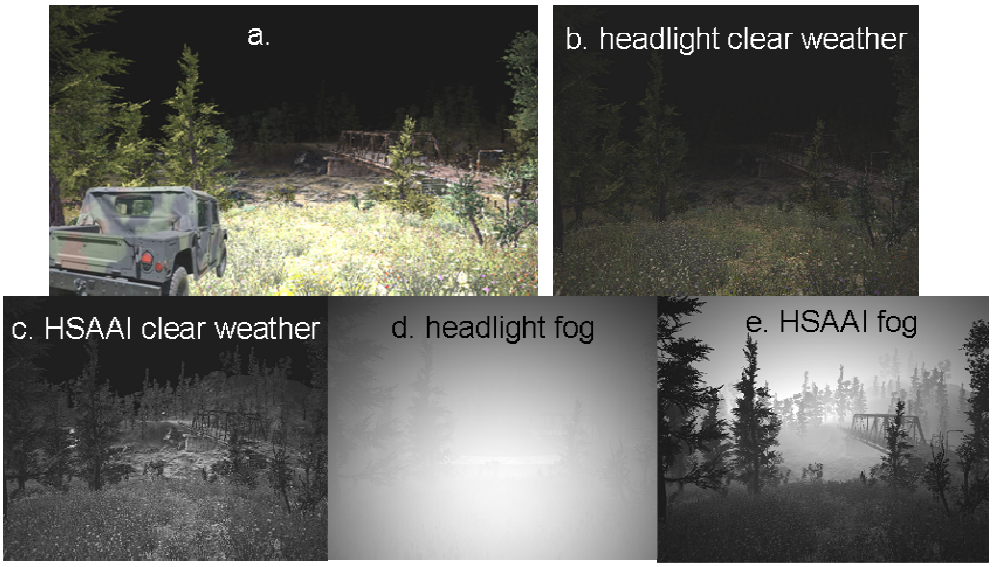

Figure 2. The driver in 2a is trying to find the bridge. Figures 2b and 2c show clear weather viewing with headlights and HSAAI respectively. Figure 2d and 2e show headlight and HSAAI viewing when in

heavy fog. Note that, although the near terrain is darker in the HSAAI image, a very long range gate is provided even in fog.

This paper provides an introduction to the HSAAI active imager. Early sections of the paper describe function and applications. Later sections describe design details.

Section Headings:

1. **Hardware Description**
2. **HSAAI Imaging Characteristics**
3. **Potential HSAAI Applications**
4. **HSAAI Range Performance**
5. **Heterodyne Discussion (no equations)**
6. **Heterodyning and Range-Gate Logic**
7. **Maturity of CMOS Technology used in HSAAI**
8. **Why No Speckle in HSAAI?**
9. **Signal to Noise Calculations**
10. **Many-Pulse Active Imaging**
11. **Conclusions**

Section 1: Hardware Description. Figure 1 depicts the major components of the HSAAI active imager. The HSAAI receiver consists of a lens and CMOS image array. The HSAAI illuminator consists of a laser diode, a lens or lenses, and probably also a diffuser. The laser diode has a volume Bragg grating to narrow the spectral band for heterodyning. Heterodyning requires a local oscillator signal, so there is a fiber optic connection between the HSAAI image array and the laser diode illuminator. Of course, both the illuminator and imager require electronics that are not shown

The HSAAI image array can be fabricated in any silicon foundry using CMOS waveguide technology. Multiple versions of each component used in the HSAAI design have been fabricated and tested, and the CMOS processes and test results are described in the open literature.

Laser diode illuminators are small, power efficient, and easy to drive. Further, the addition of a volume Bragg Grating narrows the diode spectrum sufficiently to heterodyne within the temporal bandwidth of available germanium photo detectors. All of the component parts of a HSAAI active imager are light weight, compact, power efficient, and producible.

Section 2: HSAAI Imaging Characteristics. Like other active imagers, HSAAI enhances vision through rain, fog, smoke, and other atmospheric obscurants. Like other active imagers, HSAAI provides range to objects in the imager field of view. Unlike other active imagers, HSAAI enhances poor weather vision over very long range gates. Poor weather HSAAI video has more in common with clear weather passive video than with typical active imagery.

The gated illumination sequence used by HSAAI is different from previous active imagers, and that makes HSAAI image characteristics different. For one thing, HSAAI forms completely incoherent images without any trace of speckle. A second advantage is that the low peak power pulses make HSAAI Class 1 eye safe with small emitting apertures. Another advantage is that HSAAI provides very long range gates with the ability to tailor apparent illumination versus range.

The HSAAI advantages described in the previous paragraph result from many-pulse active imaging. Summing many laser pulses to generate one video frame leads to long exposure times, and sunlit backgrounds would limit the performance of a direct detection imager. Heterodyning solves that problem. The reasons that heterodyne detection is relatively immune to sunlit backgrounds are explained later.

Two examples illustrate HSAAI imaging characteristics. Figure 2a shows an off road vehicle with the driver trying to find an old bridge to cross a ravine. The view out the windshield on a clear night using headlights is illustrated in 2b. The clear weather night view from HSAAI is shown in 2c. If it is foggy, however, the backscatter from headlights almost completely obscures the naked–eye view ahead; that is illustrated in 2d. Figure 2e shows the HSAAI image when viewing in heavy advective fog. The near terrain is darker in the HSAAI image in order to avoid excessive light backscatter from the fog.

Simulated views using a Rancher's & Farmer's Flashlight provide another example of HSAAI operation. Of course, security guards, police, and soldiers guarding aircraft on a tarmac also use flashlights. The R&F Flashlight **is** illustrated in Figure 3.

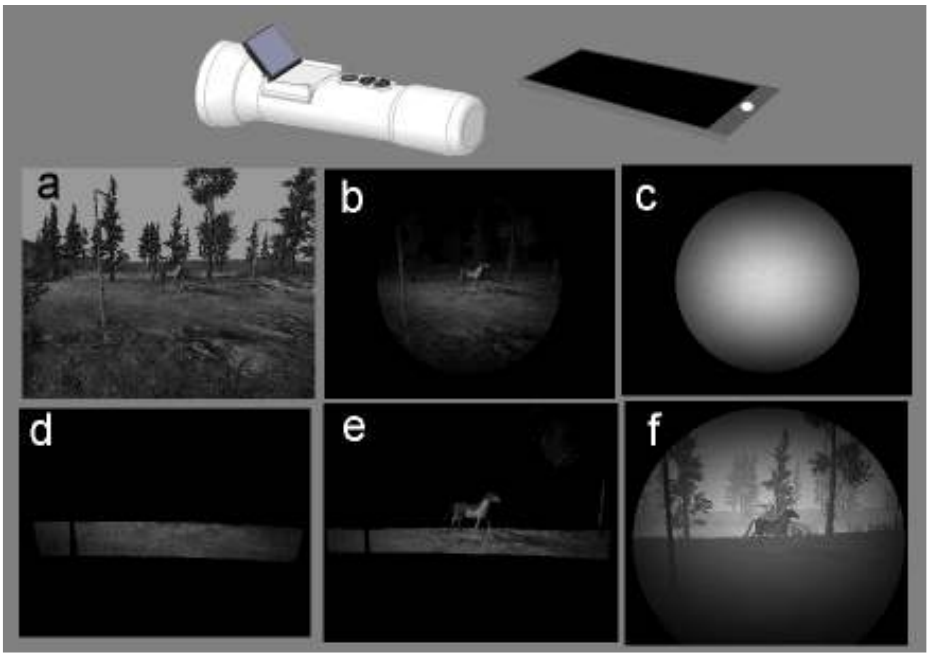

Figure 3. Image illustrating flat illumination (a), flashlight in clear weather (b), flashlight in fog (c), short range-gate active imaging (d and e), and HSAAI in fog (f).

Figure 3a shows a scene using flat illumination. The scene is lit using a ordinary flashlight in 3b. The near-range terrain is very bright and that obscures the distant scene. Figure 3c shows the view when using a flashlight in dense fog; the scene is not visible because of backscatter from the fog. A traditional active imager would gate out the

backscatter from the fog. That is illustrated in 3d and 3e, where the range gate has been changed to find the horse. HSAAI illuminates the scene differently from traditional active imagers, see Figure 3f. HSAAI reduces the near-range illumination so that back-scatter does not obscure the distant scene. In almost all cases, however, all ranges receive some illumination either directly from the illuminator or from backscattered light.

Section 3: Potential HSAAI Applications. Operation at any wavelength between 0.4 and 2 microns is supported by CMOS waveguide technology using silicon or silicon nitride waveguides and silicon or germanium photo detectors. It is likely that many applications would benefit by operating in the mid wave infrared beyond three microns. However, operation beyond two microns wavelength requires incorporating photo detectors via processes that are not universally available in CMOS foundries, and that complication is not addressed in this paper.

HSAAI are small enough to be used for missile or ordinance end game tracking and fusing. That application is illustrated in Figure 4a. HSAAI are cheap enough to be used on ground vehicles in combination with a passive wake-up sensor for threat location. That application is illustrated in Figure 4b. HSAAI also have the range performance needed for long range target acquisition in those scenarios where active imaging is acceptable. See Figure 4c.

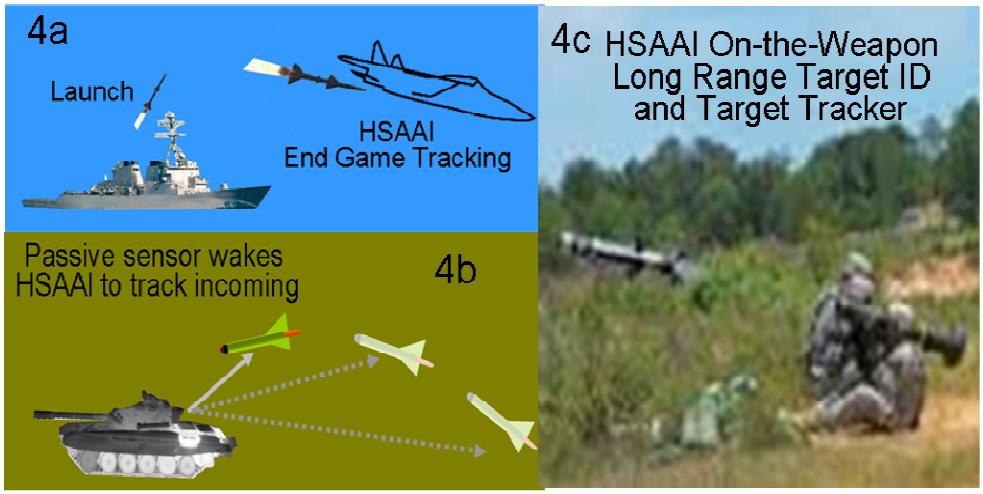

Figure 4. Some potential HSAAI applications. In Figure 4a, HSAAI provides end game target tracking and fusing. In 4b, HSAAI is paired with passive thermal for threat warning, threat location, and possibly threat elimination. In 4c, the HSAAI missile seeker pairs with a ground-mounted thermal imager for long range target identification (ID) and then performs missile in-flight target tracking.

Section 4: HSAAI Range Performance. Some specific camera designs were selected in order to illustrate expected ranges for a given combination of field of view, atmospheric transmission, and illuminator power. In all cases, the illuminator powers listed are for 120 Hertz video. However, viewing performance and pixel signal to noise is based on just one 0.008 second frame, and ranging uses the image data from two consecutive frames, but ranges are updated every frame. See "Signal to Noise Calculations" for the equations used.

Fig. 5 is provided as an aid in understanding model results. The figure shows the effect of noise on apparent image quality. From the left, the pixel signal to noise is 4:1, 2:1, 1:1, and 1:2. A pixel signal to noise of 1:2 (that is, signal to noise equals 0.5) is a useable image.

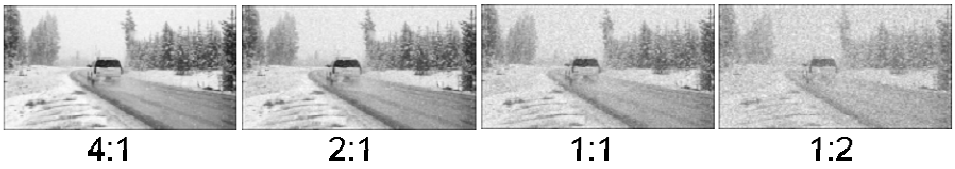

Figure 5. Labels under pictures give pixel signal to noise ratio.

HSAAI camera parameters are given in Table 1. The camera has an F/1 optic with a 30 degree field of view; the imager is suitable as a forward looking driving aid or the R & F Flashlight. The peak laser diode power is a half watt, but the average power emitted by the illuminator is just 0.1 watt.

The range predictions in Figure 6 are for atmospheric transmission of 0.2 per kilometer; that transmission is associated with heavy advective fog. The maximum range in Figure 6 is 300 meters. The modeled target has 0.2 Lambertian contrast and a one square meter area. At 300 meters range, the pixel signal to noise of two presents a clear picture to the observer. Standard deviation of range error at 300 meters is five meters for a 1.0 square meter target.

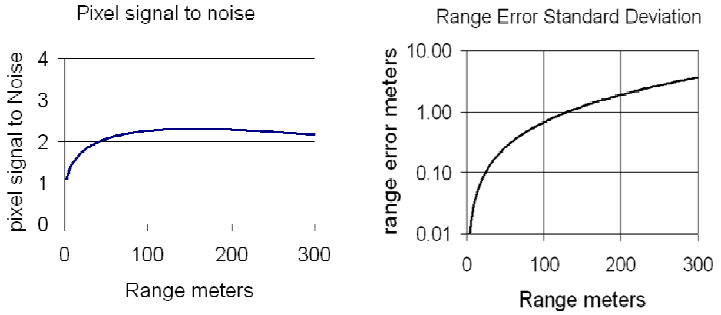

Figure 6. Range predictions for a 30 degree field of view with 3:4 vertical to horizontal aspect ratio. Conditions are heavy advective fog with transmission per kilometer of 0.2. At 300 meters range, an emitted power of 0.1 watts provides a pixel signal to noise of 2.0 and a range error of 5 meters at 300 meters range.

Table 1. Parameters used to model HSAAI range performance.

Parameter	Value	Remarks
Number of Pixels	1024 by 768	
Pixel Pitch	15 microns	
Wavelength	1.3 microns	
Spectral Bandwidth	< 0.3 nm	60 GHz Germanium Detector
Local Oscillator Power	1E-10 watts/detector	
Fill Factor	0.64	
Heterodyne Efficiency	0.5	
Coupling efficiency	0.75	
Optical Transmission	0.8	
Frame Rate	120 Hz.	Performance based on one frame
Target Reflectivity	0.3	
Background reflectivity	0.2	

HSAAI design is a compromise between photo detector pitch (image array size) and power used to achieve a specific level of performance. For example, the same performance shown in Figure 6 is achieved by changing the pitch to 30 microns and lowering the peak

power required of the laser diode illuminator from a half watt to 0.1 watt. The average emitted power for 120 Hz. video drops from 0.1 watt to 20 milliwatts.

Figure 7 shows range predictions for a two degree, F/3 optic using the Table 1 camera parameters. The maximum range plotted is now four kilometers. Atmospheric transmission per kilometer is 0.85, and the target is a 10 square meter tank. The target contrast remains 0.2. Using a four watt peak laser diode operated at 50% duty cycle, the pixel signal to noise at four kilometers is two, and the standard deviation of range error is about seven meters.

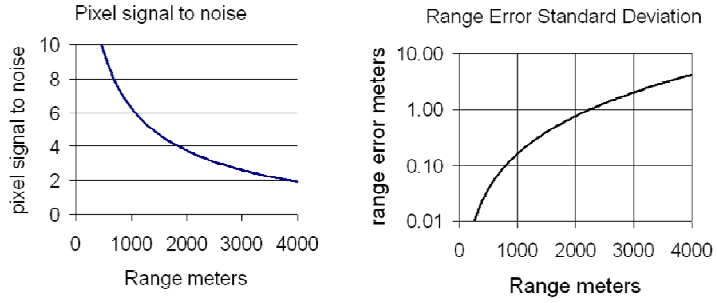

Figure 7. Range performance for an F/3 optic with two degree field of view and with clear atmosphere. Maximum range is four kilometers. Laser diode power into the beam is two watts for 120 Hertz video.

Section 5: Heterodyne Discussion (without equations). The heterodyne process described in this paper is not the multiplication of two monochromatic sine waves described in most literature. Both the illuminator light and even the local oscillator light have significant spectral bandwidth.

Referring to Figure 8, a square law photo detector multiplies the two light streams A and B. By Fourier Transform Theory, a multiplication in time is a convolution in the frequency domain, so the multiplication creates the difference temporal spectrum C in the photo diode electrical output signal.

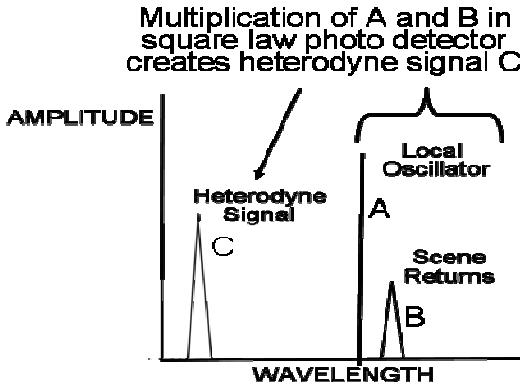

Figure 8. Plot of local oscillator (A), illuminator (B), and heterodyne (C) frequencies.

Figure 9 shows the local oscillator relative to sunlight on the detector. The average weighted wavelength of the sunlight spectrum E is indicated by the dashed line. The difference between the local oscillator D and sunlight wavelength is much greater than will pass the temporal bandwidth of the photo detector. Also, the local oscillator wavelength is inside the sun spectral band, so that light to one side of the local oscillator cancels signal from the other side. Sunlight will generate a signal F, but it will not heterodyne efficiently.

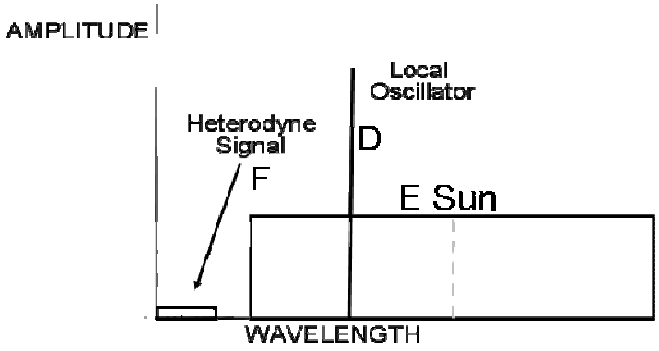

Figure 9. Sunlight does not heterodyne efficiently because the spectral band is large and the local oscillator is inside the spectrum.

Section 6: Heterodyning and Range-Gate Logic Implementation. Figure 10 illustrates the major sections of a HSAAI array.

The HSAAI pixels consist of a two dimensional array of light collection sites (LCS). Each LCS contains a light coupler 14 and a polarization diversifier 31 converting input light to a single mode in waveguide 19. Local oscillator light 17 enters via waveguide 18 and the two light streams are combined in a waveguide prior to entering a square law photo detector 7. The detector processing is labeled 26.

See the top right corner of Figure 10 for some details describing detector signal processing. The photo detector signal is AC coupled, rectified by MOMS diodes, and then integrated. After a frame consisting of many laser pulses is integrated, the LCS signal is read by row column logic, and then the integrator is reset.

The receive logic must be desensitized during illuminator emission to avoid bright backscatter and establish the illumination profiles illustrated in Figures 2 and 3. Desensitizing is accomplished by shifting the local oscillator wavelength so that the heterodyne signal is outside the temporal bandwidth of the photo detector. Keeping the local oscillator on but shifting wavelength avoids a strong level shift accompanying each gating cycle.

Also on the HSAAI image array is a set of spectral filters each consisting of multiple ring or racetrack resonators. The spectral filters are used to generate the local oscillator signal. The spectral filters are fabricated with PIN diodes inserted in the waveguides or surrounding material in order to control refractive index by passing a current through the PIN diode. In other words, the resonance wavelengths of the spectral filters is controlled by varying the current in the PIN diodes using current mirrors.

A small fraction of the illuminator signal is conveyed by fiber optic link to the image array. The illuminator light enters Spectral Filter 1 (SF1) at node 1 (the Add waveguide). Light that resonates in SF1 will exit the filter at node 2. Light that does not resonate will be fed to the photo diode at node 3. The edge of the illuminator spectral band is found by varying the current in SF1 and monitoring the photo diode signal.

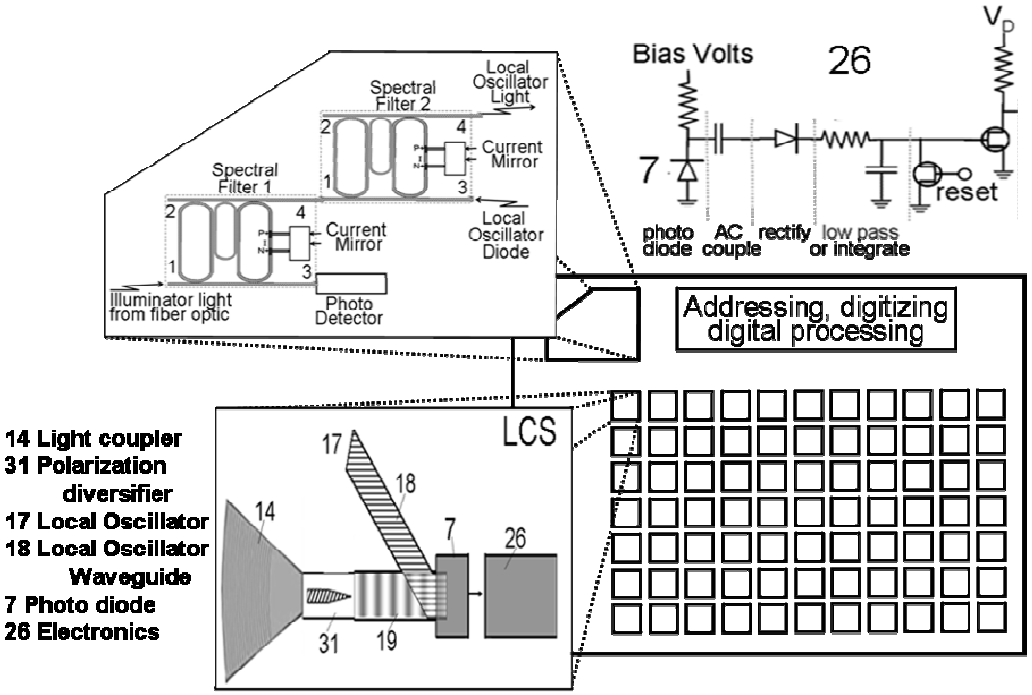

Figure 10 showing the various component parts of a HSAAI image array.

Once the wavelength of SF1 is set, the illuminator is turned off, and the local oscillator laser diode is turned on. The local oscillator light enters SF2 via node 3. The current in SF2 is varied until the amplitude on the photo detector is nulled (or minimized), and that state indicates that the local oscillator signal at node 4 of SF2 is correct.

Section 7: Maturity of CMOS Technology used in HSAAI. Although HSAAI requires process development in order to combine individual component designs into a functioning imager, the ability to fabricate each component part has been demonstrated in CMOS foundries.

Waveguide engineering has matured over the last two decades. Light in waveguides can be split and combined efficiently [1,2]. Researchers have found ways for waveguides to turn sharp corners without radiating [7], and experience suggests that laying one waveguide over another at right angles will not lead to coupling. Nano tubes etched on top of waveguides controls waveguide mode [8], and several optical mode converters have been demonstrated [9-11].

Very fast Germanium photo detectors have been integrated with waveguides [12,13]. Mach Zehnder Interferometers can be used as optical switches, and techniques with even better wavelength discrimination have been developed [14]. Both Bragg Gratings [15] and J-couplers [16,17] are used to couple light into waveguide structures. Both Quantum Dot (QD) and Graphene photo detectors have now been interfaced to silicon waveguides [18-22]; Graphene has demonstrated a 20 GHz bandwidth. Alternatives to Germanium are desirable because of the high dark current, low shunt resistance, and high burst noise of Germanium detectors [12,13].

Section 8: Why No Speckle in HSAAI? HSAAI integrates many laser pulses to form an image. The number of pulses decreases with increased maximum range setting to one pulse

at 1.2 million meters in an 0.008 second frame. At five kilometers, for example, 2400 pulses are summed, and even more are summed at closer range. Figure 11 shows the speckle reduction benefit of adding five pulses. Based on experience, summing eight pulses eliminates speckle.

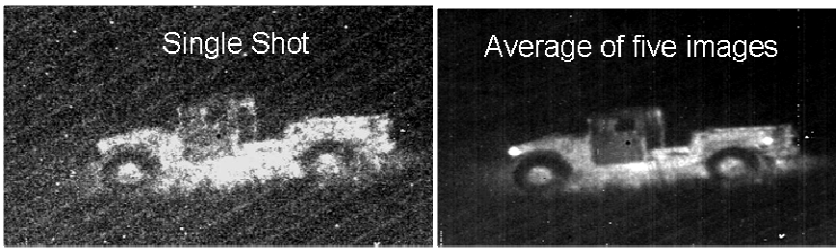

Figure 11. The picture at left shows the speckle in an image created from a single laser pulse. The reduced speckle at right results from summing five images.

Section 9: Signal to Noise Calculations. The active irradiance in photons per centimeter squared (cm^2) per second (P_{cm2}) is given by

$$P_{cm2} = \frac{watt}{e_P \, FOV_h \, FOV_v \, R_{ng}^2}. \qquad 1$$

The photo-electrons per second in each photo detector is

$$PE = \frac{P_{cm2} \, A_{trn} \, \tau \, FF \, H_e \, R_{tgt} \, QE \det^2}{4 \, F_{num}^2}. \qquad 2$$

The heterodyne signal generated in a second by PE photo-electrons is

$$E_{het} = \sqrt{2 \, PE \, e_P \, LO} \, / \, e_P. \qquad 3$$

Photo detector noise in electrons for one second is given by Eq. 4

$$P_{noi} = \sqrt{T_{frm} \{[(\frac{4 \, k \, T}{R_{shunt}})^{0.5} (\frac{1}{e^-})]^2 + D_{rk} + \frac{S_{photons} \, \Delta\lambda_D \, \tau \, QE \det^2}{4 \, F_{num}^2} + QE \, LO / e_P \}}. \qquad 4$$

The signal to noise in a frame time T_{frm} is

$$Signal / Noise = E_{het} \sqrt{T_{frm}} \Big/ P_{noi} \qquad 5$$

Equations 1 through 4 use the following definitions. I_{eff} will be explained in the next section.

watt	Emitted power in watts	LO	watts per detector
R_{ng}	Range in meters	E_{het}	Heterodyne efficiency
FOV_h	Horizontal FOV	$S_{photons}$	Sun photons/cm^2/second/micron
FOV_v	Vertical FOV	I_{eff}	Integrator efficiency
e_P	Energy per photon	H_e	Heterodyne efficiency
QE	Quantum Efficiency	A_{trn}	Atmospheric transmission

FF	Area fill factor	R_{tgt}	Target reflectivity
τ	optics transmission	det	Photo detector size in cm
F_{num}	Optics F number	drk	Photo detector dark current
R_{shunt}	Detector shunt resistance	k	Boltzman's Constant
T	FPA temperature Kelvin	$\Delta\lambda_D$	Spectral filter bandwidth in microns

Section 10: Many-pulse Range Gated Imaging. The many-pulse concept is illustrated in Figure 12. The focal plane array (FPA) is desensitized during laser emission and is turned on as the leading edge of the light pulse returns from maximum range. The FPA integrates the return light for as long as the light pulse lasts and is then desensitized (local oscillator wavelength changed) in preparation for the next laser pulse. Because laser diodes put out very little energy per pulse, many pulses are summed to provide an adequate display signal. Typically, the FPA must integrate hundreds of laser pulses before outputting a frame of video.

Figure 13. illustrates FPA gating; it diagrams the relationship between laser emission, FPA integration, and FPA read out. Display occurs after many repetitions of the laser pulse-FPA integration cycle.

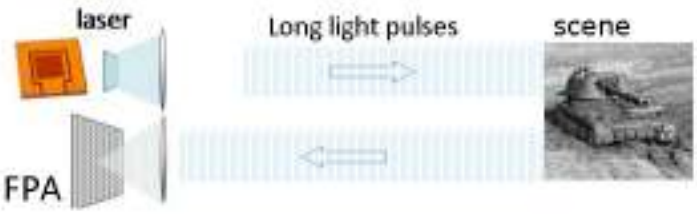

Figure 12. The FPA is gated off (that is, the heterodyne signal is not integrated) when light is being emitted by the illuminator. When light returns from R_{max}, the illuminator is turned off, and the FPA integrates signal.

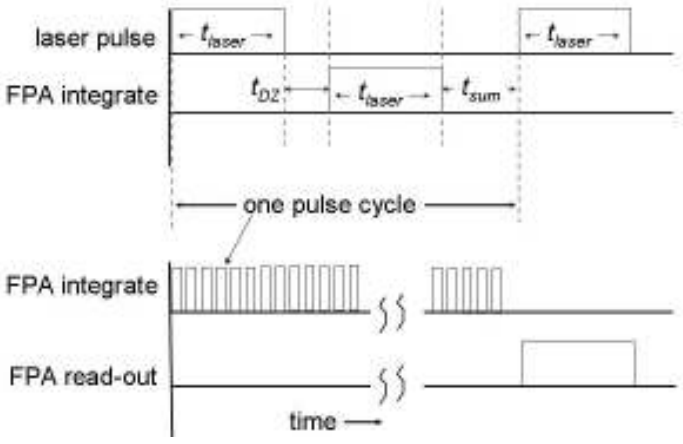

Figure 13. The top diagram shows the relationship between laser emission and signal integration. The bottom diagram shows multiple repetitions of the top sequence along with the timing of FPA read out. t_{laser} is the duration of the laser pulse; t_{DZ} is the delay between the end of the laser pulse and the beginning of light integration by the FPA; t_{sum} is a small circuit delay.

The duration of the laser pulse is set by

$$t_{laser} = \frac{2(R_{\max} - R_{DZ})}{c} \qquad 6$$

where c is the speed of light. R_{max} is the longest effective range for a particular operating environment. R_{max} is set by the observer and depends on field conditions. R_{DZ} is a dark zone that is needed to limit the dynamic range of the imager and to avoid light scattered by nearby airborne particulates. It is created by the delay t_{DZ} between the end of the laser light pulse and the beginning of FPA light integration.

Since R_{DZ} can be varied pulse-by-pulse, any apparent illumination versus range can be obtained for ranges less than R_{max}. The HSAAI FPA must desensitize during illuminator emission while shielding the signal integrated up to that point in time. Also, the FPA must transition quickly from desensitized to integrating signal in order to range at close distances.

To find range to pixel, a frame is taken per the description above, a second frame might taken without laser emission, and a third frame is taken while reducing pulse duty cycle from full to zero during the frame. Given heterodyne detection, probably only frames 1 and 3 are necessary. See Fig. 7 for an example of how pulse duty cycle is reduced over the frame time. Range is then given by Eq. 7 where I_{F1}, I_{F2}, and I_{F3} are the pixel intensities for frames one through three, respectively. Range to object of a specified size is found by convolving over the number of pixels subtended by the object.

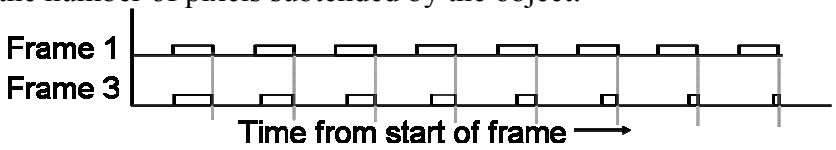

Figure 14. The laser pulse duty cycle in Frame 1 is established by the desired dark zone and maximum range. In Frame 3, the laser pulse duty cycle is gradually reduced over the frame time from full to zero.

$$R_{pix} = \frac{I_{F1} - I_{F3} - \frac{1}{2} I_{F2}}{I_{F1} - I_{F2}} 2 R_{\max} \qquad 7$$

Section 11: Conclusions. HSAAI is an active imager that uses a CMOS focal plane and laser diode illuminator. HSAAI implements heterodyne sensing in a staring array format. The benefit of heterodyne sensing is that it raises weak signals above system and background noises; in particular, HSAAI functioning is not affected by sunlit backgrounds. HSAAI provides range-to-pixel and range-gated viewing through atmospheric obscurants both day and night.

The considerable research done over the last two decades to develop silicon waveguide communications systems provides the technology needed to implement HSAAI. Because of that research, HSAAI can be fabricated in any silicon foundry. A CMOS receiver together with low peak power CW (continuous wave) laser diodes as illuminators makes a HSAAI based active imager practical economically as well as small, eye safe, and highly power efficient.

The practicality of HSAAI CMOS fabrication is supported by published research. All of the required pieces and component parts have been demonstrated. Many of the pieces like splitters, mode converters, and photo detectors can be fabricated using published process notes. Some aspects of HSAAI like the LCS light coupler have not been fabricated in exactly the form needed by HSAAI, but like parts have been fabricated.

The paper provides two examples showing practical range performance for moderate laser diode illumination powers. Just as importantly as performance, the HSAAI size, weight, and power are all quite small.

The performance advantage of HSAAI is that gated imaging and ranging do not require short range gates, and the long range gates are available day or night because heterodyning is not affected by sunlight. In some applications, short range gates are a benefit, and it is possible for HSAAI to image with a short gate. However, for applications like driving aids, terrain avoidance, and target search and acquisition, short range gates are a hindrance and not a benefit. HSAAI provides the benefits of gated imaging to view distant targets through obscurants while maintaining the ability to view intervening terrain and objects. HSAAI provides an economical solution for many applications.

References

1. Koji Yamada, "Silicon Photonic Wire Waveguides: Fundamentals and Applications," in *Silicon Photonics II,* D.J. Lockwood, L. Pavesi Eds., Topics in Applied Physics **119**, 1-19 (2011)
2. Zhe Xiao, Xianshu Luo, Peng Huei Lim, Patinharekandy Prabhathan, Samson T. H. Silalahi, Tsung-Yang Liow, Jing Zhang, and Feng Luan,"Ultra-compact low loss polarization insensitive silicon waveguide splitter," Optics Express, **21**, 10196-10203 (2013)
3. Athansios Papoulis, *The Fourier Integral and Its Applications*, (McGraw-Hill, New York, 1962), Chap. 2
4. Joseph W. Goodman, *Statistical Optics,* (John Wiley & Sons, New York, 1985), Chap 5
5. A. Sanchez, J. C. F. Davis, K. C. Liu, and A. Javan, "The MOM tunneling diode: theoretical estimate of its performance at microwave and infrared frequencies," J. Appl. Phys. **49**, 5270-5277 (1978)
6. Yanbin An, Aniruddh Shekhawat, Aghkan Behnam, Eric Pop, ant Ural, "Gate tunneling current and quantum capacitance in metal-oxide-semiconductor diodes with graphine gate electrodes," Applied Physics Letters, 223104 (2016)
7. C. Ma, Q. Zhang, and E. Van Keuren, "Right-angle slot waveguide bends with high bending efficiency," Optics Express, **16**, 14330-14334 (2008)
8. Zhaoyi Li, Myoung-Hwan Kim, ChengWang, Zhaohong Han, Sajan Shrestha, Adam Christopher Overvig, Ming Lu, Aaron Stein, Anuradha Murthy Agarwal, Marko Lončar, and Nanfang Yu, "Controlling propagation and coupling of waveguide modes using phase-gradient metasurfaces," Nature Nanotechnology, **12**, 675-683 (2017)
9. A. Xie, L. Zhou, J. Chen, and X. Li, "Efficient silicon polarization rotator based on mode-hybridization in a double-stair waveguide," Optics Express **23**, 3960-3970 (2015)
10. J. Zhang, Tsung-Yang Liow, M. Yu, Guo-Qiang Lo, and Dim-Lee Kwong, "Silicon waveguide based TE mode converter," Optics Express **18**, 25264-25270 (2010)
11. Y. Xiong, Dan-Xia Xu, J. H. Schmid, P. Cheben, S. Janz, and W. N. Ye, " Robust Silicon Waveguide Polarization Rotator With an Amorphous Silicon Overlayer," IEEE Photonics Journal **6**, 2200308 (2014)
12. C. T. DeRose, D. C. Trotter, W. A. Zortman, A. L. Starbuck, M. Fisher, M. R. Watts, and P. S. Davids, "Ultra compact 45 GHz CMOS compatible Germanium waveguide photodiode with low dark current," Optics Express **25**, 24897-22804 (2011)
13. H. Chen, P. Verheyen, P. De Heyn, G. Lepage, J. De Coster, S. Balakrishnan, P. Absil, W. Yao, L. Shen, G. Roelkens, and J. Van Campenhout,"-1 V bias 67 GHz bandwidth Si-contacted Germanium waveguide p-i-n photodetector for optical links at 56 Gbps and beyond," Optics Express **24**, 4622-4621 (2016)
14. Linjie Zhou, Richard Soref, and Jianping Chenm "Wave;engtth-selective switching using double-ring resonators coupled by a three-waveguide directional coupler," Optics Express **23**, 13488-13498 (2015)
15. Xu Wang, Samantha Grist, Jonas Flueckiger, Nicolas A. F. Jaeger, and Lukas Chrostowski, "Silicon photonic slot waveguide Bragg gratings and resonators," Optics Express **21**, 19029-19039 (2013)
16. Thomas Dillan, Janusz Murakowski, Shouyuan Shi, and Dennis Prather, "Fiber-to-waveguide coupler based on the parabolic reflector," Optics Letters **33**, 896-898 (2008)
17. Maifuz Ali and Seong-Ook Park, "Analysis of Horn Antennas in Receiving Mode as an EM Field Sensor," Hindawi International Journal of Antennas and Propagation, Vol. 2012, Article ID 134916, (2012)
18. Yating Wan, Zeyu Zhang, Ruilin chao, Justin Norman, Daewan Jung, Chen Shang, Qiang Li, M.J. Kennedy, Di Liang, Chong Zhang, Jin-Wei Shi, Arthur C. Gossard, Kei May Lau, and John e. Bowers, "Monolithically integrated InAs/InGaAs quantum dot photodetectors on silicon substrates," Optics Express **25**, 749-753 (2017)
19. F. H. L. Koppens, T. Mueller, Ph. Avouris, A. C. Ferrari, M. S. Vitiello and M. Polini, "Photodetectors based on graphene, other two-dimensional materials and hybrid systems," nature nanotechnology **9**, 780-793 (2014)
20. Gan, X. *et al.* Chip-integrated ultrafast graphene photodetector with high responsivity, Nature Photon. **7**, 883–887 (2013)
21. Pospischil, A. *et al.* "CMOS-compatible graphene photodetector covering all optical communication bands," Nature Photon. 7, 892–896 (2013)
22. Wang, X., Cheng, Z., Xu, K., Tsang, H. K., Xu, J. "High-responsivity graphene/silicon-heterostructure waveguide photodetectors, Nature Photon. 7, 888–891 (2013)
23.http://www.me.umn.edu/courses/me8254/attfiles/Lecture%2007%20Dry%20Etching_Full.pdf
24.http://web.ece.ucdavis.edu/~anayakpr/Papers/Wet%20and%20Dry%20Etching_submitted.pdf

25. https://pdfs.semanticscholar.org/6a89/67e0ed9f35122bf7205a2dc414872da9d2e7.pdf